Fall 2020-21, Senior Project I – Final Report

Numerical Simulation of Geometric Squeezing in Rotating Bose-Einstein Condensates

Kadir Çeven

December 27, 2020

Abstract

This project aims to find an efficient numerical method to reproduce the recent experiment from Martin Zwierlein's group [15] on Bose-Einstein condensates in an elliptically confined trap which results in geometric squeezing. This requires to solve the Gross-Pitaevskii equation for rotating BECs. For this, the ground state of rotating BECs in harmonic traps are calculated by applying the multigrid preconditioned Polak–Ribière–Polyak conjugate gradient method as suggested in [12]. This method is tested with some analytic properties related to BECs. In the last part of this project, reproducing the results of the related experiment is focused.

Contents

1 Dimensionless GPE for Rotating BECs

The Hamiltonian for rotating BECs in 2D is

$$\hat{\mathbf{H}}_\psi = \frac{-\hbar^2}{2m}\Delta + \hat{\mathbf{V}}(\mathbf{r}) + g\,|\psi(\mathbf{r})|^2 - \Omega\,\hat{\mathbf{L}}_z(\mathbf{r}) \tag{1}$$

where $\hat{\mathbf{V}}(\mathbf{r}) = \frac{1}{2}m(\omega_x^2 x^2 + \omega_y^2 y^2)$ for a harmonic potential and $\hat{\mathbf{L}}_z(\mathbf{r}) = -i\hbar\left(x\frac{\partial}{\partial y} - y\frac{\partial}{\partial x}\right)$ for the z-component of angular momentum.

The GPE for rotating BECs is

$$\hat{\mathbf{H}}_\psi\, \psi(\mathbf{r}) = \mu\, \psi(\mathbf{r}) \tag{2}$$

where the chemical potential μ is

$$\mu = \frac{\langle\psi|\hat{\mathbf{H}}_\psi|\psi\rangle}{\langle\psi|\psi\rangle} \tag{3}$$

and the constraint is

$$\langle\psi|\psi\rangle = \|\psi\|_2^2 = \int_{\mathbb{R}^2} |\psi(\mathbf{r})|^2 \mathrm{d}x\, \mathrm{d}y = N. \tag{4}$$

The energy functional E is

$$E(\psi) = \frac{\langle\psi|\hat{\mathbf{H}}_\psi|\psi\rangle - \frac{1}{2}g|\psi|^2\langle\psi|\psi\rangle}{\langle\psi|\psi\rangle}. \tag{5}$$

For numerical purposes, all of these equations need to be dimensionless so let's define ℓ as in Eq. (6).

$$\ell = \sqrt{\frac{\hbar}{m\omega_x}} \tag{6}$$

Let also $\tilde{x}$ and $\tilde{y}$ be as defined in Eq. (7) and (8), respectively.

$$\tilde{x} \equiv \frac{x}{\ell} \tag{7}$$

$$\tilde{y} \equiv \frac{y}{\ell} \tag{8}$$

The constraint in Eq. (4) becomes

$$\langle\psi|\psi\rangle = \int_{\mathbb{R}^2} |\psi(\tilde{\mathbf{r}})|^2 \mathrm{d}\tilde{x}\, \mathrm{d}\tilde{y}\, \ell^2 = N. \tag{9}$$

To make Eq. (9) fully dimensionless, let $\tilde{\psi}(\tilde{\mathbf{r}})$ be as in Eq. (10).

$$\tilde{\psi}(\tilde{\mathbf{r}}) \equiv \ell\, \psi(\mathbf{r}) \tag{10}$$

By inserting Eq. (10) into Eq. (9), the constraint becomes Eq. (11).

$$\langle\tilde{\psi}|\tilde{\psi}\rangle = \int_{\mathbb{R}^2} |\tilde{\psi}(\tilde{\mathbf{r}})|^2 \mathrm{d}\tilde{x}\, \mathrm{d}\tilde{y} = N \tag{11}$$

To also make $\hat{\mathbf{H}}_\psi$ dimensionless, we insert Eq. (7), (8) and (10) into Eq. (1).

$$\hat{\mathbf{H}}_\psi = \frac{-\hbar^2}{2m}\frac{1}{\ell^2}\left(\frac{\partial^2}{\partial\tilde{x}^2} + \frac{\partial^2}{\partial\tilde{y}^2}\right) + \frac{1}{2}m\ell^2(\omega_x^2\tilde{x}^2 + \omega_y^2\tilde{y}^2) + g\frac{1}{\ell^2}|\tilde{\psi}(\tilde{\mathbf{r}})|^2 + i\,\Omega\,\hbar\left(\tilde{x}\frac{\partial}{\partial\tilde{y}} - \tilde{y}\frac{\partial}{\partial\tilde{x}}\right) \tag{12}$$

We insert Eq. (6) into Eq. (12).

$$\hat{\mathbf{H}}_\psi = \frac{-\hbar^2}{2m}\frac{m\omega_x}{\hbar}\left(\frac{\partial^2}{\partial\tilde{x}^2} + \frac{\partial^2}{\partial\tilde{y}^2}\right) + \frac{1}{2}m\frac{\hbar}{m\omega_x}(\omega_x^2\tilde{x}^2 + \omega_y^2\tilde{y}^2) + g\frac{m\omega_x}{\hbar}|\tilde{\psi}(\tilde{\mathbf{r}})|^2 + i\,\Omega\,\hbar\left(\tilde{x}\frac{\partial}{\partial\tilde{y}} - \tilde{y}\frac{\partial}{\partial\tilde{x}}\right) \tag{13}$$

$$= \frac{-\hbar\omega_x}{2}\left(\frac{\partial^2}{\partial\tilde{x}^2} + \frac{\partial^2}{\partial\tilde{y}^2}\right) + \frac{1}{2}\frac{\hbar}{\omega_x}(\omega_x^2\tilde{x}^2 + \omega_y^2\tilde{y}^2) + g\frac{m\omega_x}{\hbar}|\tilde{\psi}(\tilde{\mathbf{r}})|^2 + i\,\Omega\,\hbar\left(\tilde{x}\frac{\partial}{\partial\tilde{y}} - \tilde{y}\frac{\partial}{\partial\tilde{x}}\right) \tag{14}$$

Let's divide $\hat{\mathbf{H}}_\psi$ by $\hbar\omega_x$ and define $\tilde{\hat{\mathbf{H}}}_\psi \equiv \frac{\hat{\mathbf{H}}_\psi}{\hbar\omega_x}$, $\tilde{\Delta} \equiv \frac{\partial^2}{\partial\tilde{x}^2} + \frac{\partial^2}{\partial\tilde{y}^2}$ and $\tilde{\hat{\mathbf{L}}}_z \equiv -i\left(\tilde{x}\frac{\partial}{\partial\tilde{y}} - \tilde{y}\frac{\partial}{\partial\tilde{x}}\right)$. Thus, we get

$$\tilde{\hat{\mathbf{H}}}_\psi = \frac{-1}{2}\tilde{\Delta} + \frac{1}{2}\left(\tilde{x}^2 + \frac{\omega_y^2}{\omega_x^2}\tilde{y}^2\right) + g\frac{m}{\hbar^2}|\tilde{\psi}(\tilde{\mathbf{r}})|^2 - \frac{\Omega}{\omega_x}\tilde{\hat{\mathbf{L}}}_z. \tag{15}$$

Let γ_y, $\tilde{g}$ and $\tilde{\Omega}$ be as defined in Eq. (16), (17) and (18), respectively.

$$\gamma_y \equiv \frac{\omega_y}{\omega_x} \tag{16}$$

$$\tilde{g} \equiv g\frac{m}{\hbar^2} \tag{17}$$

$$\tilde{\Omega} \equiv \frac{\Omega}{\omega_x} \tag{18}$$

$\tilde{\hat{\mathbf{H}}}_\psi$ becomes as shown in Eq. (19) by defining $\tilde{\hat{\mathbf{V}}} \equiv \frac{1}{2}\left(\tilde{x}^2 + \gamma_y^2\tilde{y}^2\right)$.

$$\tilde{\hat{\mathbf{H}}}_\psi = \frac{-1}{2}\tilde{\Delta} + \tilde{\hat{\mathbf{V}}} + \tilde{g}|\tilde{\psi}(\tilde{\mathbf{r}})|^2 - \tilde{\Omega}\tilde{\hat{\mathbf{L}}}_z \tag{19}$$

Hence, the GPE, μ and $E(\psi)$ become as shown in Eq. (20), (21) and (22), respectively.

$$\tilde{\hat{\mathbf{H}}}_\psi\ \tilde{\psi}(\tilde{\mathbf{r}}) = \tilde{\mu}\ \tilde{\psi}(\tilde{\mathbf{r}}) \tag{20}$$

$$\tilde{\mu} = \frac{\langle\tilde{\psi}|\tilde{\hat{\mathbf{H}}}_\psi|\tilde{\psi}\rangle}{\langle\tilde{\psi}|\tilde{\psi}\rangle} \tag{21}$$

$$\tilde{E}(\tilde{\psi}) = \frac{\langle\tilde{\psi}|\tilde{\hat{\mathbf{H}}}_\psi|\tilde{\psi}\rangle - \frac{1}{2}\tilde{g}|\tilde{\psi}|^2\langle\tilde{\psi}|\tilde{\psi}\rangle}{\langle\tilde{\psi}|\tilde{\psi}\rangle} \tag{22}$$

We drop the tildes for convenience.

2 Fourier Pseudo-Spectral Discretization

Since finding a solution of the GPE for rotating BECs is analytically challenging, it is more convenient to carry out it numerically. Thus, we need to discretize the wave function ψ in 2D. Throughout this project, we use the Fourier pseudo-spectral discretization based on FFTs to speed out our calculations and to simplify our notations because $\hat{\mathbf{H}}_\psi$ is not sparse unlike in the finite element method.

Let's truncate the wave function ψ on a bounded domain $U = [-L, L]^2$. We fix the spatial mesh sizes $h_x = 2L/M_x$ and $h_y = 2L/M_y$ for two positive integers M_x and M_y. We define $x_j = -L + jh_x$ and $y_k = -L + kh_y$ for $j = 0, 1, \dots, M_x - 1$ and $k = 0, 1, \dots, M_y - 1$. Thus, the mesh wave function $\tilde{\phi}_{jk}$ becomes the numerical approximation of $\psi(x_j, y_k)$. For the Fourier space, we define the discretized Fourier frequencies $\xi_p = p\pi/L$ and $\nu_q = q\pi/L$ for $p = -M_x/2, \dots, 0, \dots, M_x/2 - 1$ and $q = -M_y/2, \dots, 0, \dots, M_y/2 - 1$. Hence,

$$\mathcal{O}_{M_x,M_y} = \left\{\ (j,k) \in \mathbb{N}^2 \mid 0 \leqslant j \leqslant M_x - 1,\ 0 \leqslant k \leqslant M_y - 1\ \right\} \tag{23}$$

$$\tilde{\mathcal{O}}_{M_x,M_y} = \left\{\ (p,q) \in \mathbb{Z}^2 \mid -M_x/2 \leqslant p \leqslant M_x/2 - 1,\ -M_y/2 \leqslant q \leqslant M_y/2 - 1\ \right\} \tag{24}$$

$$\mathcal{D}_{xy} = \left\{\ (x_j, y_k) = (-L + jh_x, -L + kh_y) \mid (j,k) \in \mathcal{O}_{M_x,M_y}\ \right\} \tag{25}$$

$$\tilde{\mathcal{D}}_{\xi\nu} = \left\{\ (\xi_p, \nu_q) = (p\pi/L, q\pi/L) \mid (p,q) \in \tilde{\mathcal{O}}_{M_x,M_y}\ \right\} \tag{26}$$

The Fourier coefficients in the x- and y- directions are

$$\hat{\tilde{\phi}}_{pk} = \sum_{j=0}^{M_x-1} \tilde{\phi}_{jk} \exp\left(-i\xi_p(x_j - L)\right) \tag{27}$$

$$\hat{\tilde{\phi}}_{jq} = \sum_{k=0}^{M_y-1} \tilde{\phi}_{jk} \exp\left(-i\nu_q(y_k - L)\right). \tag{28}$$

Thus, the pseudo-spectral approximations in the x- and y- directions are

$$\tilde{\phi}_{jk} = \frac{1}{M_x} \sum_{p=-M_x/2}^{M_x/2-1} \hat{\tilde{\phi}}_{pk} \exp\left(i\xi_p(x_j - L)\right) \tag{29}$$

$$\tilde{\phi}_{jk} = \frac{1}{M_y} \sum_{q=-M_y/2}^{M_y/2-1} \hat{\tilde{\phi}}_{jq} \exp\left(i\nu_q(y_k - L)\right). \tag{30}$$

By applying the operators $\frac{\partial^2}{\partial x^2}$, $\frac{\partial^2}{\partial y^2}$, $y\frac{\partial}{\partial x}$ and $x\frac{\partial}{\partial y}$ to $\tilde{\phi}_{jk}$, we find out

$$\frac{\partial^2}{\partial x^2}\tilde{\phi}_{jk} = \frac{1}{M_x} \sum_{p=-M_x/2}^{M_x/2-1} (-\xi_p^2)\, \hat{\tilde{\phi}}_{pk} \exp\left(i\xi_p(x_j - L)\right) \tag{31}$$

$$\frac{\partial^2}{\partial y^2}\tilde{\phi}_{jk} = \frac{1}{M_y} \sum_{q=-M_y/2}^{M_y/2-1} (-\nu_q^2)\, \hat{\tilde{\phi}}_{jq} \exp\left(i\nu_q(y_k - L)\right) \tag{32}$$

$$y\frac{\partial}{\partial x}\tilde{\phi}_{jk} = \frac{1}{M_x} \sum_{p=-M_x/2}^{M_x/2-1} i\xi_p y\, \hat{\tilde{\phi}}_{pk} \exp\left(i\xi_p(x_j - L)\right) \tag{33}$$

$$x\frac{\partial}{\partial y}\tilde{\phi}_{jk} = \frac{1}{M_y} \sum_{q=-M_y/2}^{M_y/2-1} i\nu_q y\, \hat{\tilde{\phi}}_{jq} \exp\left(i\nu_q(y_k - L)\right). \tag{34}$$

3 Numerical Methods

After choosing a certain type of discretization, we can attempt to find numerical solutions of the GPE which is the discrete minimization problem in Eq. (35).

$$\phi_g = \arg\min_{\phi \in \mathcal{S}} E(\phi) \tag{35}$$

where $\mathcal{S} = \left\{ \phi \mid \|\phi\|_2^2 = N,\ E(\phi) < \infty \right\}$.

The classical methods in [8] come from the theory of partial differential equations which are based on the imaginary time equation in Eq. (36).

$$\frac{\partial}{\partial t}\phi = -\hat{\mathbf{H}}_\phi \phi \tag{36}$$

The time discretization with Δt can be done by using Forward Euler, Backward Euler, or Crank-Nicolson methods. When Δt is small enough, $E(\phi)$ decreases; however, it does not preserve the constraint in Eq. (11).

Therefore, we need a constrained minimization method without free parameters like Δt to carry out efficient numerical calculations. For this, [12] suggests the following gradient methods.

3.1 Preconditioned Gradient Method (PG)

In the preconditioned gradient method, the following update needs to be carried out for Eq. (35).

$$\tilde{\phi}_{n+1} = \phi_n - \alpha_n P \left(\hat{\mathbf{H}}_{\phi_n} \phi_n - \mu_n \phi_n \right) \tag{37}$$

and

$$\phi_{n+1} = \frac{\tilde{\phi}_{n+1}}{\sqrt{\langle \tilde{\phi}_n, \tilde{\phi}_n \rangle}} = \frac{\tilde{\phi}_{n+1}}{\|\tilde{\phi}_{n+1}\|_2} \tag{38}$$

where $\mu_n = \langle \hat{\mathbf{H}} \phi_n, \phi_n \rangle / \|\phi_n\|_2^2 = \langle \hat{\mathbf{H}} \phi_n, \phi_n \rangle / N$.

Alternatively, Eq. (37) and (38) can be written like Eq. (39) as suggested in [12].

$$\phi_{n+1} = \cos(\theta_n)\, \phi_n + \sin(\theta_n) \frac{p_n \sqrt{N}}{\|p_n\|_2} \tag{39}$$

where $p_n = d_n - \frac{\Re\langle d_n, \phi_n \rangle}{N} \phi_n$, $d_n = -P r_n$ is the descent direction, $r_n = \hat{\mathbf{H}}_{\phi_n} \phi_n - \mu_n \phi_n$ is the preconditioned residual and $\theta_n = \alpha_n \sqrt{N} / \|p_n\|_2$. Eq. (39) is equivalent to Eq. (37) and (38) only when θ_n is small enough.

Let's expand ϕ_{n+1} in Eq. (39) around $\theta_n = 0$.

$$\begin{aligned} \phi_{n+1} &= \left(1 - \frac{\theta_n^2}{2!} + \ldots \right) \phi_n + \left(\theta_n - \frac{\theta_n^3}{3!} + \ldots \right) \frac{p_n \sqrt{N}}{\|p_n\|_2} \\ &= \phi_n + \theta_n \frac{p_n \sqrt{N}}{\|p_n\|_2} - \frac{\theta_n^2}{2} \phi_n + \mathcal{O}(\theta_n^3) \end{aligned} \tag{40}$$

and thus

$$\begin{aligned} E(\phi_{n+1}) &= E(\phi_n) + \frac{\theta_n \sqrt{N}}{\|p_n\|_2} \Re\langle \nabla E(\phi_n), p_n \rangle + \frac{1}{2} \theta_n^2 \left(\frac{\nabla^2 E(\phi_n)[p_n, p_n] N}{\|p_n\|_2^2} - \Re\langle \nabla E(\phi_n), \phi_n \rangle \right) + \mathcal{O}(\theta_n^3) \\ &= E(\phi_n) + \frac{\theta_n \sqrt{N}}{\|p_n\|_2} \Re\langle \nabla E(\phi_n), p_n \rangle + \frac{\theta_n^2 N}{2\|p_n\|_2^2} \left(\nabla^2 E(\phi_n)[p_n, p_n] - \frac{\Re\langle \nabla E(\phi_n), \phi_n \rangle \|p_n\|_2^2}{N} \right) + \mathcal{O}(\theta_n^3) \end{aligned} \tag{41}$$

[12, 14] suggest that

$$\langle \nabla E(\phi_n), f \rangle = \frac{\langle 2 \hat{\mathbf{H}}_{\phi_n} \phi_n, f \rangle}{N} \tag{42}$$

$$\frac{1}{2} \nabla^2 E(\phi_n)[f, f] = \frac{\langle f, \hat{\mathbf{H}}_{\phi_n} f \rangle + \Re\langle g_n, f \rangle}{N} \tag{43}$$

where $g_n = 2 g \rho_{p\phi}^n \phi_n$ with $\rho_{p\phi}^n = \Re(\phi_n \bar{p}_n)$.

Hence, Eq. (41) becomes

$$E(\phi_{n+1}) = E(\phi_n) + \frac{\theta_n \sqrt{N}}{\|p_n\|_2} \Re\langle \nabla E(\phi_n), p_n \rangle + \frac{\theta_n^2 N}{\|p_n\|_2^2} \left(\frac{1}{2} \nabla^2 E(\phi_n)[p_n, p_n] - \frac{\mu_n}{N} \|p_n\|_2^2 \right) + \mathcal{O}(\theta_n^3). \tag{44}$$

Approximately,

$$E(\phi_{n+1}) \approx E(\phi_n) + \frac{\theta_n \sqrt{N}}{\|p_n\|_2} \Re\langle \nabla E(\phi_n), p_n \rangle + \frac{\theta_n^2 N}{\|p_n\|_2^2} \left(\frac{1}{2} \nabla^2 E(\phi_n)[p_n, p_n] - \frac{\mu_n}{N} \|p_n\|_2^2 \right). \tag{45}$$

To minimize $E(\phi_{n+1})$, we need to choose such θ_n value that

$$\theta_n = \arg\min_{\theta} \phi_{n+1} = \arg\min_{\theta} \left(\cos(\theta)\, \phi_n + \sin(\theta) \frac{p_n \sqrt{N}}{\|p_n\|_2} \right). \tag{46}$$

For this minimization, the Wolfe conditions or a line search can be applied; however, there is an easier way to do that as suggested in [12, 14].

Let's take the derivative of $E(\phi_{n+1})$ in Eq. (45) with respect to θ_n and make it equal to zero so that we can find a local minimum of $E(\phi_{n+1})$ which gives Eq. (47).

$$\theta_n^{\text{opt}} = \frac{-\Re\langle \nabla E(\phi_n), p_n\rangle \|p_n\|_2}{2\sqrt{N}\left(\frac{1}{2}\nabla^2 E(\phi_n)[p_n, p_n] - \frac{\mu_n}{N}\|p_n\|_2^2\right)} \tag{47}$$

Since the minimization requires $E(\phi_{n+1}) < E(\phi_n)$, the obtained θ_n value (θ_n^{opt}) in Eq. (47) must be a candidate minimizer. Thus, we need to check θ_n^{opt} so that $\theta_n^{\text{opt}} > 0$.

Let's check the numerator of Eq. (47).

$$\begin{aligned}
-\Re\langle \nabla E(\phi_n), p_n\rangle \|p_n\|_2 &= -\Re\langle \nabla E(\phi_n), d_n - \Re\langle d_n, \phi_n\rangle \phi_n\rangle \|p_n\|_2 \\
&= -\left(\Re\langle \nabla E(\phi_n), d_n\rangle - \Re\langle \nabla E(\phi_n), \Re\langle d_n, \phi_n\rangle \phi_n\rangle\right) \|p_n\|_2 \\
&= -\left(\Re\langle \nabla E(\phi_n), d_n\rangle - \Re\langle d_n, \phi_n\rangle \Re\langle \nabla E(\phi_n), \phi_n\rangle\right) \|p_n\|_2 \\
&= -\left(2\Re\langle \hat{\mathbf{H}}_{\phi_n}\phi_n, d_n\rangle - 2\Re\langle d_n, \phi_n\rangle \Re\langle \hat{\mathbf{H}}_{\phi_n}\phi_n, \phi_n\rangle\right) \|p_n\|_2/N \\
&= -\left(2\Re\langle \hat{\mathbf{H}}_{\phi_n}\phi_n, d_n\rangle - 2\mu_n N \Re\langle d_n, \phi_n\rangle\right) \|p_n\|_2/N \\
&= -\left(2\Re\langle \hat{\mathbf{H}}_{\phi_n}\phi_n, -Pr_n\rangle - 2\mu_n N \Re\langle -Pr_n, \phi_n\rangle\right) \|p_n\|_2/N \\
&= \left(2\Re\langle \hat{\mathbf{H}}_{\phi_n}\phi_n, Pr_n\rangle - 2\mu_n N \Re\langle Pr_n, \phi_n\rangle\right) \|p_n\|_2/N
\end{aligned} \tag{48}$$

We know $\langle \phi_n, r_n\rangle = \langle r_n, \phi_n\rangle = 0$ and $P > 0$. Then,

$$\begin{aligned}
-\Re\langle \nabla E(\phi_n), p_n\rangle \|p_n\|_2 &= \left(2\Re\langle \hat{\mathbf{H}}_{\phi_n}\phi_n, Pr_n\rangle\right) \|p_n\|_2/N \\
&= \left(2\Re\langle r_n, Pr_n\rangle + 2\mu_n \Re\langle \phi_n, Pr_n\rangle\right) \|p_n\|_2/N \\
&= 2\Re\langle r_n, Pr_n\rangle \|p_n\|_2/N > 0.
\end{aligned} \tag{49}$$

Therefore, if the denominator is also positive, θ_n^{opt} is positive and the energy may decrease. If it does not decrease, we will decrease θ_n^{opt} until we get $E(\phi_{n+1}) < E(\phi_n)$.

If the denominator is negative, we choose a small positive value for θ_n^{opt}. We apply the same procedure as above until the energy decreases.

We repeat these steps until

$$\varepsilon_n^{\text{err}} = |E(\phi_{n+1}) - E(\phi_n)| < \epsilon_\varepsilon. \tag{50}$$

3.2 Preconditioned Polak–Ribière–Polyak Conjugate Gradient Method (PCG)

We use nearly the same method as above except

$$d_n = -Pr_n + \beta_n^{\text{PR}} p_{n-1} \tag{51}$$

where

$$\beta_n^{\text{PR}} = \frac{\langle r_n - r_{n-1}, Pr_n\rangle}{\langle r_{n-1}, Pr_{n-1}\rangle} \tag{52}$$

which is the Polak–Ribière–Polyak choice if $\beta_n^{\text{PR}} > 0$. Else, the PG method will be restarted once.

If $\beta_n^{\text{PR}} > 0$, we need to apply a slightly different minimization method. In this method, it is not guaranteed that the numerator of θ_n^{opt} in Eq. (47) is positive. Thus, if the numerator is positive, we choose θ_n^{opt} as in Eq. (47) without checking the denominator and apply the same step-size control as in the PG. If not, we restart the PG method once.

3.3 Preconditioners

Using preconditioners in the PG and PCG methods decreases computational cost. Hence, we need to choose them carefully so that these iterative methods converge faster.

Algorithm 1: The Preconditioned Gradient Method (PG)

$n \leftarrow 0$
while not $\varepsilon_n^{\mathrm{err}} < \epsilon_\varepsilon$ **do**
  $\mu_n \leftarrow \langle \hat{\mathbf{H}}_{\phi_n} \phi_n, \phi_n \rangle / N$
  $r_n \leftarrow \hat{\mathbf{H}}_{\phi_n} \phi_n - \mu_n \phi_n$
  $d_n \leftarrow -P r_n$
  $p_n \leftarrow d_n - \frac{\Re\langle d_n, \phi_n \rangle}{N} \phi_n$
  if $\left(\frac{1}{2} \nabla^2 E(\phi_n)[p_n, p_n] - \mu_n \|p_n\|_2^2 \right) > 0$ **then**
    $\theta_n^{\mathrm{opt}} \leftarrow \frac{-\Re\langle \nabla E(\phi_n), p_n \rangle \|p_n\|_2}{2\sqrt{N}\left(\frac{1}{2} \nabla^2 E(\phi_n)[p_n, p_n] - \frac{\mu_n}{N} \|p_n\|_2^2 \right)}$
  else
    $\theta_n^{\mathrm{opt}} \leftarrow -\Re\langle \nabla E(\phi_n), p_n \rangle \|p_n\|_2$
  end if
  while not $E(\phi_{n+1}(\theta_n^{\mathrm{opt}})) < E(\phi_n)$ or not $\theta_n^{\mathrm{opt}} < \epsilon$ **do**
    $\theta_n^{\mathrm{opt}} \leftarrow \theta_n^{\mathrm{opt}} / 2$
  end while
  $\theta_n \leftarrow \theta_n^{\mathrm{opt}}$
  $\phi_{n+1} \leftarrow \cos(\theta_n)\, \phi_n + \sin(\theta_n)\, \frac{p_n \sqrt{N}}{\|p_n\|_2}$
  $n \leftarrow n + 1$
end while

Algorithm 2: The Preconditioned Polak–Ribière–Polyak Conjugate Gradient Method (PCG)

$n \leftarrow 0$
apply the PG method once
$n \leftarrow 1$
while not $\varepsilon_n^{\mathrm{err}} < \epsilon_\varepsilon$ **do**
  $\mu_n \leftarrow \langle \hat{\mathbf{H}}_{\phi_n} \phi_n, \phi_n \rangle / N$
  $r_n \leftarrow \hat{\mathbf{H}}_{\phi_n} \phi_n - \mu_n \phi_n$
  $\beta_n^{\mathrm{PR}} \leftarrow \frac{\langle r_n - r_{n-1}, P r_n \rangle}{\langle r_{n-1}, P r_{n-1} \rangle}$
  if $\beta_n^{\mathrm{PR}} \leqslant 0$ **then**
    $\beta_n \leftarrow 0$
    apply the PG method once
  else
    $\beta_n \leftarrow \beta_n^{\mathrm{PR}}$
    $d_n \leftarrow -P r_n + \beta_n p_{n-1}$
    $p_n \leftarrow d_n - \frac{\Re\langle d_n, \phi_n \rangle}{N} \phi_n$
    if $-\Re\langle \nabla E(\phi_n), p_n \rangle \|p_n\|_2 > 0$ **then**
      $\theta_n^{\mathrm{opt}} \leftarrow \frac{-\Re\langle \nabla E(\phi_n), p_n \rangle \|p_n\|_2}{2\sqrt{N}\left(\frac{1}{2} \nabla^2 E(\phi_n)[p_n, p_n] - \frac{\mu_n}{N} \|p_n\|_2^2 \right)}$
      while not $E(\phi_{n+1}(\theta_n^{\mathrm{opt}})) < E(\phi_n)$ or not $\theta_n^{\mathrm{opt}} < \epsilon$ **do**
        $\theta_n^{\mathrm{opt}} \leftarrow \theta_n^{\mathrm{opt}} / 2$
      end while
      $\theta_n \leftarrow \theta_n^{\mathrm{opt}}$
      $\phi_{n+1} \leftarrow \cos(\theta_n)\, \phi_n + \sin(\theta_n)\, \frac{p_n \sqrt{N}}{\|p_n\|_2}$
    else
      apply the PG method once
    end if
  end if
  $n \leftarrow n + 1$
end while

3.3.1 Kinetic Energy Preconditioner

Firstly, [12] suggests the following preconditioner which uses only the kinetic energy term in the GPE

$$P_\Delta = \left(\alpha_\Delta - \frac{1}{2}\Delta\right)^{-1} \tag{53}$$

where

$$\alpha_\Delta = \tilde{\mu}_n = \frac{1}{N}\int_{\mathbb{R}^2}\left(\frac{1}{2}\phi_n^*\Delta\phi_n - \hat{\mathbf{V}}|\phi_n|^2 + g|\phi_n|^4\right)\mathrm{d}x\,\mathrm{d}y. \tag{54}$$

3.3.2 Potential Energy Preconditioner

Secondly, it suggests the following preconditioner which uses the potential energy term

$$P_V = \left(\alpha_V + \hat{\mathbf{V}} + g|\phi_n|^2\right)^{-1} \tag{55}$$

where $\alpha_V = \tilde{\mu}_n$.

3.3.3 Combined Preconditioner

By combining these two preconditioners symmetrically, we get

$$P_\mathrm{C} = P_V^{1/2} P_\Delta P_V^{1/2}. \tag{56}$$

We use this preconditioner instead of P_Δ or P_V throughout this project. Thus we call the PCG with this preconditioner P_C as the $\mathrm{PCG_C}$.

3.4 Multigrid $\mathrm{PCG_C}$ Method

Since small fixed mesh sizes – h_x and h_y – (or big grid number $M_y \times M_x$) increase computational cost enormously, we need to find another approach for the ground state to converge faster. Instead, we will use a multigrid approach as in Algorithm 3.

Algorithm 3: The Multigrid $\mathrm{PCG_C}$ Method

given p_initial and p_end
$p \leftarrow p_\mathrm{initial}$
given ϕ_0^p on $\mathcal{D}_{xy}^p$ where $M_x = M_y = 2^p$
while $p < p_\mathrm{end}$ **do**
  run Algorithm 2 with the initial state ϕ_0^p and get ϕ_g^p
  interpolate ϕ_g^p at $\mathcal{D}_{yx}^{p+1}$ and get ϕ_g^{p+1}
  $p \leftarrow p + 1$
  $\phi_0^p \leftarrow \phi_\mathrm{g}^p$
end while

4 Comparisons with the Analytical Properties

To examine the multigrid $\mathrm{PCG_C}$ method, the following analytical properties related to the GPE can be used.

4.1 Non-Interacting Case in a Rotating Trap

In the case of $g = 0$ and $N = 1$, [9] exactly gives the probability density

$$|\phi_g(x, y)|^2 = \frac{1}{\pi a_x a_y} \exp\left(-\frac{x^2}{a_x^2} - \frac{y^2}{a_y^2}\right) \tag{57}$$

where

$$a_x^2 = \frac{1 + \beta_+\beta_-}{\beta_+}\frac{1}{\gamma} \quad \& \quad a_y^2 = \frac{1 + \beta_+\beta_-}{\beta_-}\frac{1}{\gamma} \tag{58}$$

$$\beta_+ = \frac{2\Omega\omega_+}{\gamma_y^2 - \omega_+^2 - \Omega^2} \quad \& \quad \beta_- = \frac{2\Omega\omega_-}{\omega_-^2 - 1 + \Omega^2} \quad \& \quad \gamma = \frac{\sqrt{\frac{1}{4}(\gamma_y^2 - 1)^2 + 4\omega_\perp^2\Omega^2}}{\Omega} \tag{59}$$

and

$$\omega_\pm^2 = \omega_\perp^2 + \Omega^2 \mp \sqrt{\frac{1}{4}(\gamma_y^2 - 1)^2 + 4\omega_\perp^2\Omega^2} \quad \& \quad \omega_\perp^2 = \frac{1}{2}(1 + \gamma_y^2). \tag{60}$$

The energy E is

$$E = \frac{1}{2}(\omega_+ + \omega_-). \tag{61}$$

For an isotropic trap ($\gamma_y = 1$), $a_x = 1$ and $a_y = 1$. Hence, $E = 1$.

We take $N = 1$, $g = 0$, $\Omega = 0.99$, $\gamma_y = 1$, $p_{initial} = 6$, $p_{end} = 8$, $L = 5$, $\epsilon_\varepsilon = 10^{-12}$ and the initial wave function is chosen as a normalized random state.

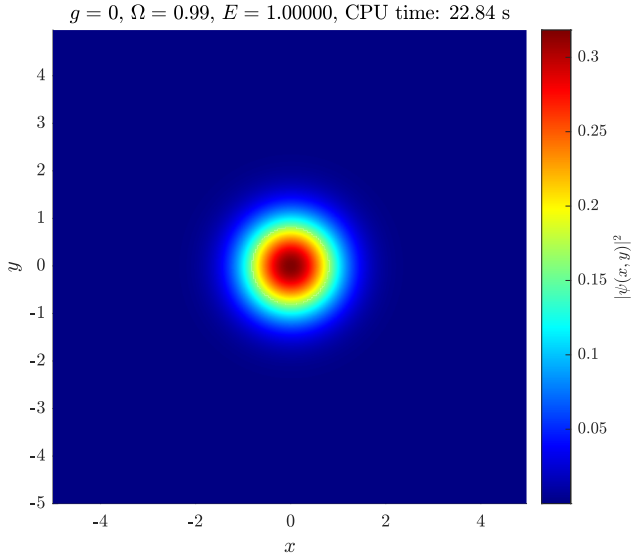

Figure 1: Plot of the non-interacting case in the rotating trap with $N = 1$, $g = 0$, $\Omega = 0.99$, $\gamma_y = 1$, $p_{initial} = 6$, $p_{end} = 8$, $L = 5$ and $\epsilon_\varepsilon = 10^{-12}$.

Figure 1 and 2 confirm that the numerical solution is the same as the wave function in Eq. (57).

4.2 Interacting Case in a Rotating Trap

In this case, we use the lowest Landau level (LLL) approximation. This approximation is only valid if the trap rotates enough (*i.e.* $\Omega \to 1$) and the below restriction is considered.

For the comparison, [7] defines a reduced energy, which must be minimized as follows.

$$E(\phi) = \frac{E_{\mathrm{LLL}}(\phi) - \Omega}{1 - \Omega} = \int_{\mathbb{R}^2} \left((x^2 + y^2)|\phi|^2 + \frac{\Lambda}{2}|\phi|^4\right) \mathrm{d}x\,\mathrm{d}y \tag{62}$$

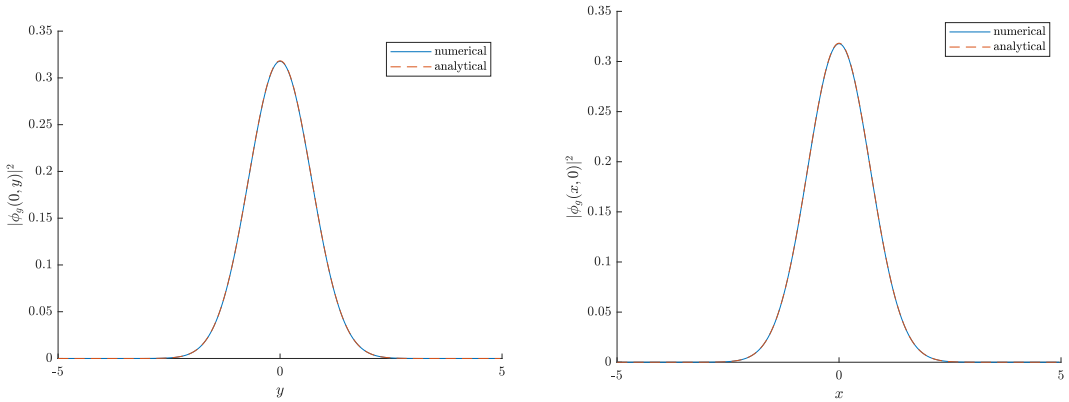

(a) $|\phi_g(0,y)|^2$ (b) $|\phi_g(x,0)|^2$

Figure 2: Plots of $x = 0$ and $y = 0$ slices of Figure 1 with their analytical results.

where

$$\Lambda = \frac{g}{1-\Omega} \tag{63}$$

Both [7, 9] obtain the following density distribution for a symmetric trap ($\gamma_y = 1$)

$$|\phi_g(x,y)|^2 = \frac{2}{\pi R_0^2}\left(1 - \frac{x^2+y^2}{R_0^2}\right) \tag{64}$$

where

$$R_0 = \left(\frac{2\Lambda}{\pi}\right)^{1/4}. \tag{65}$$

Then, [7] gets the following two minimized reduced energies

$$E_{\min_1} = \frac{2\sqrt{2}}{3\sqrt{\pi}}\sqrt{\Lambda} \tag{66}$$

and

$$E_{\min_2} = \frac{2\sqrt{2}}{3\sqrt{\pi}}\sqrt{b\Lambda} \tag{67}$$

where $b = 1.1596$ is the numerical value for a triangular Abrikosov vortex lattice.

It also indicates a restriction to the LLL if

$$g(1-\Omega) \ll 1 \tag{68}$$

To see whether the restriction to the LLL approximation is valid, it should result in a big error in the numerical simulations if $g(1-\Omega)$ is much greater than 1.

In the numerical simulations, we use the following the initial states as suggested in [12]

$$\begin{aligned}
\phi_a(x,y) = \frac{1}{\sqrt{\pi}}\exp\left(-0.5(x^2+y^2)\right) \quad \& \quad \phi_b(x,y) = (x+iy)\phi_a(x,y) \quad \& \quad \phi_{\bar{b}}(x,y) = \bar{\phi}_b(x,y) \\
\phi_c(x,y) = \frac{0.5(\phi_a(x,y)+\phi_b(x,y))}{\|0.5(\phi_a(x,y)+\phi_b(x,y))\|_2} \quad \& \quad \phi_{\bar{c}}(x,y) = \bar{\phi}_c(x,y) \\
\phi_d(x,y) = \frac{(1-\Omega)\phi_a(x,y)+\Omega\phi_b(x,y)}{\|(1-\Omega)\phi_a(x,y)+\Omega\phi_b(x,y)\|_2} \quad \& \quad \phi_{\bar{d}}(x,y) = \bar{\phi}_d(x,y) \\
\phi_e(x,y) = \frac{\Omega\phi_a(x,y)+(1-\Omega)\phi_b(x,y)}{\|\Omega\phi_a(x,y)+(1-\Omega)\phi_b(x,y)\|_2} \quad \& \quad \phi_{\bar{e}}(x,y) = \bar{\phi}_e(x,y)
\end{aligned} \tag{69}$$

and we choose the calculated ground state that has the lowest energy because of the minimization problem in Eq. (35).

Table 1: Numerical and approximated energies for different $g(1-\Omega)$ values.

Ω	$g(1-\Omega)$	E_{num}	E_{LLL_1}	% error	E_{LLL_2}	% error
0.1	27	2.34216	2.86395	-18.22	3.07636	-23.87
0.5	15	2.34216	2.56013	-8.51	2.71844	-13.84
0.6	12	2.34182	2.44264	-4.13	2.58424	-9.38
0.7	9	2.24182	2.29577	-2.35	2.41840	-7.30
0.8	6	2.12058	2.10294	0.84	2.20307	-3.74
0.9	3	1.86371	1.82132	2.33	1.89212	-1.50
0.99	0.3	1.30273	1.28135	1.67	1.30374	-0.08

For $N = 1$, $g = 30$, $\gamma_y = 1$, $p_{initial} = 6$, $p_{end} = 8$, $L = 8$ and $\epsilon_\varepsilon = 10^{-12}$, the numerical results are as follows.

The table shows that both LLL approximations are restricted by $g(1-\Omega) \ll 1$ to approximate the ground state well. Besides, the superior is the second approximation in Eq. (67), which agrees with [7].

Moreover, let's look at $x = 0$ and $y = 0$ slices of the density distribution for $g = 30$ and $\Omega = 0.99$.

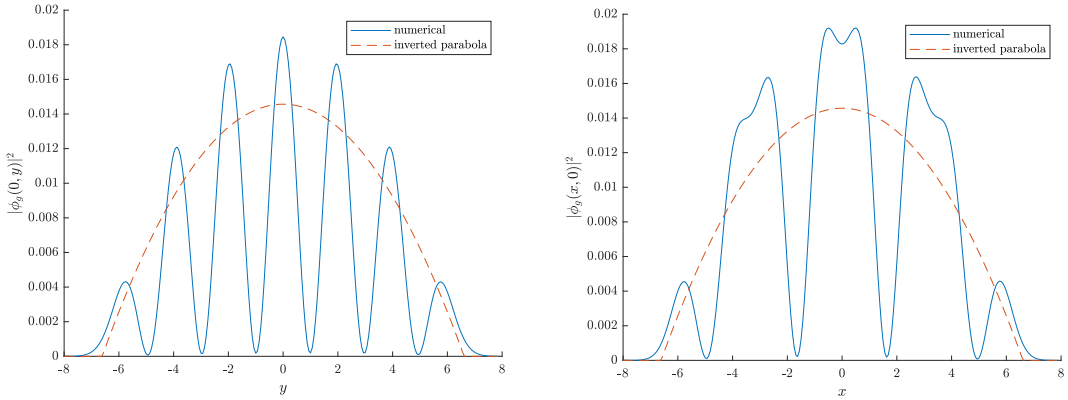

(a) $|\phi_g(0,y)|^2$ (b) $|\phi_g(x,0)|^2$

Figure 3: Plots of $x = 0$ and $y = 0$ slices of the density distribution for $g = 30$ and $\Omega = 0.99$ with their analytical approximations.

Figure 3 shows that these slices correlate with the density distribution in Eq. (64) as expected.

4.3 Feynman Relation

In a rotating superfluid, the dependence of the number of vortices $N_{\text{V}}^{\text{lattice}}$ as a function of the rotation frequency Ω and the average angular momentum per atom all over the condensate $\langle \ell_z/\hbar \rangle$ have been studied in [2, 3, 6].

The number of vortices $N_{\text{V}}^{\text{lattice}}$ can be found in the limit of a rigid-body rotation by Feynman's rule

$$N_{\text{V}}^{\text{lattice}} = \mathcal{A}_{\text{c}} n_{\text{V}} \tag{70}$$

where $\mathcal{A}_{\text{c}}$ is the area of condensate and $n_{\text{V}} = \frac{2\Omega}{\kappa}$ is the mean vortex density with $\kappa = \frac{2\pi\hbar}{m}$.

Since $\mathcal{A}_{\text{c}} = \pi R^2$ where R is the condensate radius,

$$N_{\text{V}}^{\text{lattice}} = \frac{m\Omega R^2}{\hbar}. \tag{71}$$

Moreover, it is known that $\langle \ell_z/\hbar \rangle$ depends on the number of vortices $N_{\text{V}}^{\text{lattice}}$ due to the lattice formation [3]. Hence, an approach to ℓ_z can lead us to find $N_{\text{V}}^{\text{lattice}}$ approximately as in [6].

Let's assume that the probability density of non-normalized wave function is the mean vortex density, *i.e.*, $|\phi(x,y)|^2 = n_{\text{V}}$ and $\ell_z = m\Omega(x^2+y^2)$. The average angular momentum per atom all over the condensate can

be found as

$$\begin{aligned}\langle \ell_z/\hbar \rangle &= \frac{\int_{\mathbb{R}^2} |\phi(x,y)|^2 (\ell_z/\hbar)\, \mathrm{d}x\, \mathrm{d}y}{\left[\right] \int_{\mathbb{R}^2} |\phi(x,y)|^2\, \mathrm{d}x\, \mathrm{d}y \big] / N} \\ &= \frac{N \int_0^{2\pi} \int_0^R \left(\frac{m\Omega}{\pi\hbar}\right) \left(\frac{m\Omega r^2}{\hbar}\right) r\, \mathrm{d}r\, \mathrm{d}\theta}{\int_0^{2\pi} \int_0^R \left(\frac{m\Omega}{\pi\hbar}\right) r\, \mathrm{d}r\, \mathrm{d}\theta} \\ &= \frac{\frac{N m^2 \Omega^2 R^4}{2\hbar^2}}{\frac{m\Omega R^2}{\hbar}} \\ &= \frac{N m \Omega R^2}{2\hbar}.\end{aligned} \tag{72}$$

Thus, Eq. (71) and (72) give the following relation

$$\frac{\langle \ell_z/\hbar \rangle}{N} = \frac{N_{\mathrm{V}}^{\mathrm{lattice}}}{2}. \tag{73}$$

To numerically test the relation in Eq. (73), we compute the ground states for $g = 100$, $\gamma_y = 1$ and $\Omega \in [0.40, 0.95]$. The other parameters are $N = 1$, $p_{initial} = 6$, $p_{end} = 9$, $L = 10$ and $\epsilon_\varepsilon = 10^{-12}$.

Concerning Feynman's relation, the relation in Eq. (73) can be tested by counting vortices for each rotation frequency Ω.

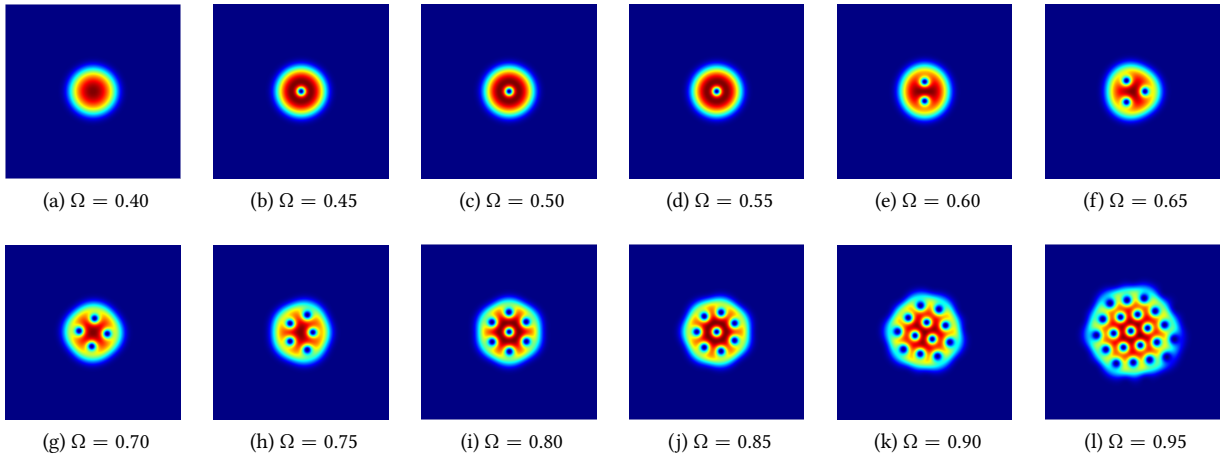

(a) $\Omega = 0.40$ (b) $\Omega = 0.45$ (c) $\Omega = 0.50$ (d) $\Omega = 0.55$ (e) $\Omega = 0.60$ (f) $\Omega = 0.65$

(g) $\Omega = 0.70$ (h) $\Omega = 0.75$ (i) $\Omega = 0.80$ (j) $\Omega = 0.85$ (k) $\Omega = 0.90$ (l) $\Omega = 0.95$

Figure 4: Plots of the ground state density $|\phi(x,y)|^2$ for $g = 100$, $\gamma_y = 1$ and $\Omega \in [0.40, 0.95]$.

Figure 5 show that the numerical results sufficiently confirm Eq. (73). A slight discrepancy appears possibly due to the inhomogeneous density.

Another problem in Figure 5 is that the calculation of $\langle \ell_z/\hbar \rangle$ is made by the numerical results so it is not an exact comparison of numerical and theoretical results. There are some theoretical approximations as in [11], however, they are only valid for a combination of a harmonic oscillator plus optical lattice.

5 Geometric Squeezing in a Rotating BEC

In 2019, Martin Zwierlein's group have experimentally observed geometric squeezing in rotating BECs which results in the LLL [15]. For this, they first prepare a ground state of rotating BEC of ^{23}Na atoms in a TOP trap and then apply the saddle potential $\hat{\mathbf{V}}_S$ at $\tilde{\Omega} = 1$.

To simulate this system, we need to reduce the 3D GPE to a 2D GPE effectively so that we can determine dimensionless parameters. With these parameters, we find the ground state and then make the state evolve in time with the time-splitting spectral method (TSSP) [5, 8] after applying $\hat{\mathbf{V}}_S$.

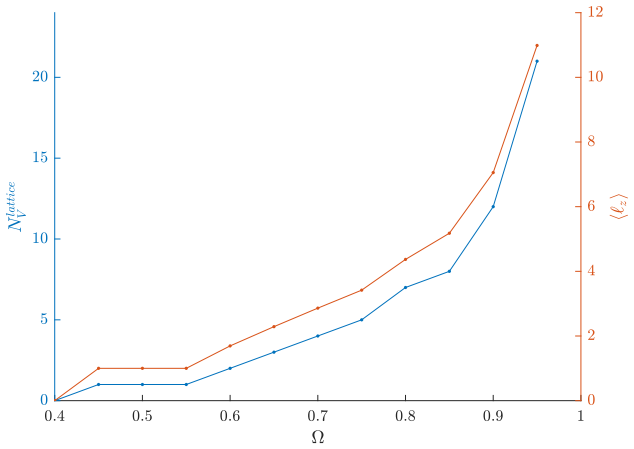

Figure 5: Plots of $N_{\mathrm{V}}^{\mathrm{lattice}}$ vs. Ω and $\langle \ell_z \rangle$ vs. Ω for $N = 1$, $g = 100$ and $\gamma_y = 1$.

5.1 Reduction of the 3D GPE to a 2D GPE

Since the experiment is carried out with a strongly interacting Bose gas, we can use the Thomas-Fermi approximation to determine the 2D coupling constant (κ_2) approximately.

The Thomas-Fermi approximation in 3D suggests that the wave function for $\kappa_3 \gg 1$ can be taken as [5, 10]

$$\tilde{\phi}_{\mathrm{g}}^{\mathrm{TF}}(\tilde{\mathbf{r}}) = \begin{cases} \sqrt{\frac{\tilde{\mu}_{\mathrm{g}}^{\mathrm{TF}} - \tilde{\tilde{\mathbf{V}}}_3(\tilde{\mathbf{r}})}{\kappa_3}}, & \text{if } \tilde{\tilde{\mathbf{V}}}_3(\tilde{\mathbf{r}}) \leqslant \tilde{\mu}_{\mathrm{g}}^{\mathrm{TF}} \\ 0, & \text{otherwise} \end{cases} \tag{74}$$

where

$$\tilde{\mu}_{\mathrm{g}}^{\mathrm{TF}} = \frac{1}{2}\left(\frac{15\kappa_3\gamma_y\gamma_z}{4\pi}\right)^{2/5}, \tag{75}$$

$$\tilde{\tilde{\mathbf{V}}}_3(\tilde{\mathbf{r}}) = \frac{1}{2}\left(\tilde{x}^2 + \gamma_y^2\tilde{y}^2 + \gamma_z^2\tilde{z}^2\right) \tag{76}$$

and

$$\kappa_3 = \frac{4\pi a_s N_{\mathrm{a}}}{\ell}. \tag{77}$$

By supposing that we deal with a disk-shaped condensate with small height *i.e.*, $\gamma_y \approx 1$ and $\gamma_z \gg 1$ [5], the 3D GPE becomes a reduced GPE which equals

$$\tilde{\mu}\tilde{\psi}_2(\tilde{x},\tilde{y}) = -\frac{1}{2}\Delta\tilde{\psi}_2(\tilde{x},\tilde{y}) + \tilde{\tilde{\mathbf{V}}}_2(\tilde{x},\tilde{y})\tilde{\psi}_2(\tilde{x},\tilde{y}) + \kappa_2|\tilde{\psi}_2(\tilde{x},\tilde{y})|^2\tilde{\psi}_2(\tilde{x},\tilde{y}) \tag{78}$$

where

$$\int_{\mathbb{R}^2} |\tilde{\psi}_2(\tilde{x},\tilde{y})|^2 \,\mathrm{d}\tilde{x}\,\mathrm{d}\tilde{y} = 1, \tag{79}$$

$$\tilde{\tilde{\mathbf{V}}}_2(\tilde{x},\tilde{y}) = \frac{1}{2}\left(\tilde{x}^2 + \gamma_y^2\tilde{y}^2\right) \tag{80}$$

and

$$\kappa_2 = \kappa_3 \int_{\mathbb{R}} |\tilde{\psi}_3(z)|^4 \mathrm{d}\tilde{z}. \tag{81}$$

For condensates with strong repulsive interaction, [5] gives $\tilde{\psi}_3(\tilde{z})$ as

$$\tilde{\psi}_3(\tilde{z}) \approx \sqrt{\int_{\mathbb{R}^2} |\tilde{\phi}_{\mathrm{g}}^{\mathrm{TF}}(\tilde{\mathbf{r}})|^2 \,\mathrm{d}\tilde{x}\,\mathrm{d}\tilde{y}}. \tag{82}$$

After inserting Eq. (82) into Eq. (81), we find [5]

$$\kappa_2 = \kappa_3 \int_{\mathbb{R}} |\tilde{\psi}_3(z)|^4 \mathrm{d}\tilde{z}. \tag{83}$$

Because the defined constraint in Eq. (11) is not as in Eq. (79), κ_2 will be different from $\tilde{g}$ in Eq. (17). It turns out that

$$\kappa_2 = N\tilde{g} \tag{84}$$

Hence, the constraint value N and the coupling constant $\tilde{g}$ in our simulations are

$$N = (N_{\mathrm{a}})^{4/5} \tag{85}$$

and

$$\tilde{g} = \frac{5}{7}\left(\frac{4\pi}{15\gamma_y}\right)^{1/5}\left(\frac{\gamma_z\kappa_3}{N_{\mathrm{a}}}\right)^{4/5}. \tag{86}$$

5.2 Finding the Ground State

The parameters of the experiment are given explicitly in [15]. To find the ground state, we need to make these parameters dimensionless.

They are $N_a = 8.1 \times 10^5$, $m = 3.818 \times 10^{-26}$ kg [13], $a_s = 3.307$ nm [1], $\omega_x = \omega_y = 2\pi \times 88.6$ Hz, $\omega_z = \sqrt{8}\omega_x$ [10] and $\Omega = 0.8\omega_x$. They correspond to $N = (8.1 \times 10^5)^{4/5}$, $\gamma_y = 1$, $\gamma_z = \sqrt{8}$, $\tilde{g} = 6.552 \times 10^{-2}$ and $\tilde{\Omega} = 0.8$. In addition to these, we also need to define a bounded domain $U = [-L, L]^2$, p_{initial}, p_{end} and ϵ_ε. Considering the given Thomas-Fermi radius of 21 µm $\approx 9.428\ell$, $L = 20$ is an appropriate choice because the major radius of the condensate increases and its minor radius decrease during the squeezing process. We also choose p_{initial}, p_{end} and ϵ_ε as 6, 9 and 10^{-12}, respectively. We drop the tildes for convenience.

By initializing the multigrid PCG_{C} method with the initial wave functions in Eq. (69), we find that the initial wave ϕ_a gives the state that has the lowest energy, *i.e.*, a feasible ground state for those parameters as shown in Table 2.

Table 2: Calculated energies of the ground state for $N = (8.1 \times 10^5)^{4/5}$, $\gamma_y = 1$, $\gamma_z = \sqrt{8}$, $g = 6.552 \times 10^{-2}$, $\Omega = 0.8$, $L = 20$, $p_{\text{initial}} = 6$, $p_{\text{end}} = 9$ and $\epsilon_\varepsilon = 10^{-12}$ with the initial wave functions in Eq. (69).

	ϕ_a	ϕ_b	$\phi_{\bar{b}}$	ϕ_c	$\phi_{\bar{c}}$	ϕ_d	$\phi_{\bar{d}}$	ϕ_e	$\phi_{\bar{e}}$
$E(\phi)$	**14.6124**	14.6133	14.6124	14.6130	14.6126	14.6126	14.6129	14.6124	14.6127
CPU time (s)	**2288.48**	3783.61	2123.76	2549.59	1979.57	1868.03	1760.75	1868.49	1671.87

5.3 Applying the Saddle Potential $\hat{\mathbf{V}}_S$ at $\Omega = 1$

In the experiment, the next step is to apply an additional potential – the saddle potential $\hat{\mathbf{V}}_S$

$$\hat{\mathbf{V}}_S = \frac{1}{2}\varepsilon(x^2 - y^2) \tag{87}$$

where ε is the trap ellipticity, which is taken as 0.125 at $\Omega = 1$ for a time duration of $0.4/\zeta$ ($\zeta = \varepsilon/2$).

For the dynamics of the condensate, we use the time-splitting spectral method (TSSP) [5, 8]. By this method, we solve the following time-dependent GPE

$$i\frac{\partial}{\partial t}\Psi(x, y, t) = (\hat{\mathbf{H}}_1 + \hat{\mathbf{H}}_2)\Psi(x, y, t) \tag{88}$$

where $\Psi(x, y, t)$ is the 2D time-dependent wave function, $\hat{\mathbf{H}}_1 = -\frac{1}{2}\Delta - \Omega\hat{\mathbf{L}}_z$ and $\hat{\mathbf{H}}_2 = \hat{\mathbf{V}}_2 + \hat{\mathbf{V}}_S + g|\Psi(x, y, t)|^2$. This equation can be solved from $t = t_n$ to $t = t_{n+1}$ (n = 0, 1, 2, ...) by splitting into three steps. Thus, let's define the time step $\Delta t = t_{n+1} - t_n > 0$ then $t_n = n\Delta t$. First, we solve

$$i\frac{\partial}{\partial t}\Psi(x, y, t) = \hat{\mathbf{H}}_{1x}\Psi(x, y, t) = \left(-\frac{1}{2}\frac{\partial^2}{\partial x^2} - i\Omega y\frac{\partial}{\partial x}\right)\Psi(x, y, t) \tag{89}$$

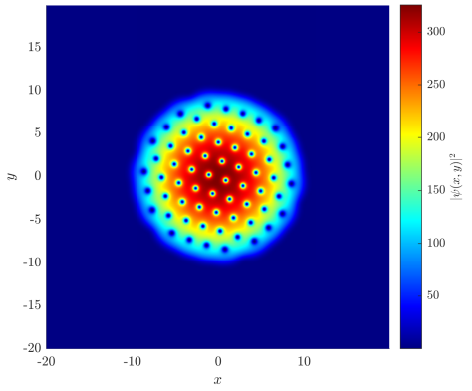

Figure 6: Plot of the density function $|\phi(x,y)|^2$ of the ground state of rotating BEC for $N = (8.1 \times 10^5)^{4/5}$, $\gamma_y = 1$, $\gamma_z = \sqrt{8}$, $g = 6.552 \times 10^{-2}$, $\Omega = 0.8$, $L = 20$, $p_{\text{initial}} = 6$, $p_{\text{end}} = 9$ and $\epsilon_\varepsilon = 10^{-12}$ with the initial wave function of ϕ_a.

for Δt, followed in solving

$$i\frac{\partial}{\partial t}\Psi(x,y,t) = \hat{\mathbf{H}}_{1y}\Psi(x,y,t) = \left(-\frac{1}{2}\frac{\partial^2}{\partial y^2} + i\Omega x\frac{\partial}{\partial y}\right)\Psi(x,y,t) \tag{90}$$

for the same Δt, followed in solving

$$i\frac{\partial}{\partial t}\Psi(x,y,t) = \hat{\mathbf{H}}_2\Psi(x,y,t) = \left(\hat{\mathbf{V}}_2 + \hat{\mathbf{V}}_S + g|\Psi(x,y,t)|^2\right)\Psi(x,y,t) \tag{91}$$

for the same Δt. By combining the splitting steps in Eq. (89), (90) and (91) with the Strang splitting [5, 8], Ψ_{jk}^{n+1} (discretized $\Psi(x,y,t_{n+1})$) is calculated as follows

$$\begin{aligned}
\Psi_{jk}^{*} &= \frac{1}{M_x}\sum_{p=-M_x/2}^{M_x/2-1}\exp\left[-i\frac{\Delta t}{2}\left(\frac{1}{2}\xi_p^2 + \Omega y\xi_p\right)\right]\widehat{\Psi}_{pk}^{n}\exp\left(i\xi_p(x_j - L)\right)\\
\Psi_{jk}^{**} &= \frac{1}{M_y}\sum_{q=-M_y/2}^{M_y/2-1}\exp\left[-i\frac{\Delta t}{2}\left(\frac{1}{2}\nu_q^2 - \Omega x\nu_q\right)\right]\widehat{\Psi}_{jq}^{*}\exp\left(i\nu_q(y_j - L)\right)\\
\Psi_{jk}^{***} &= \exp\left[-i\Delta t\left(\hat{\mathbf{V}}_2 + \hat{\mathbf{V}}_S + g|\Psi_{jk}^{**}|^2\right)\right]\Psi_{jk}^{**}\\
\Psi_{jk}^{****} &= \frac{1}{M_y}\sum_{q=-M_y/2}^{M_y/2-1}\exp\left[-i\frac{\Delta t}{2}\left(\frac{1}{2}\nu_q^2 - \Omega x\nu_q\right)\right]\widehat{\Psi}_{jq}^{***}\exp\left(i\nu_q(y_j - L)\right)\\
\Psi_{jk}^{n+1} &= \frac{1}{M_x}\sum_{p=-M_x/2}^{M_x/2-1}\exp\left[-i\frac{\Delta t}{2}\left(\frac{1}{2}\xi_p^2 + \Omega y\xi_p\right)\right]\widehat{\Psi}_{pk}^{****}\exp\left(i\xi_p(x_j - L)\right).
\end{aligned} \tag{92}$$

We apply the TSSP in Eq. (92) to the previously calculated ground state with the parameters of $N = (8.1 \times 10^5)^{4/5}$, $\gamma_y = 1$, $\gamma_z = \sqrt{8}$, $g = 6.552 \times 10^{-2}$, $\Omega = 1$, $\varepsilon = 0.125$, $L = 20$, $p = 9$ and $\Delta t = 0.001$ from the time $t = 0$ to $t = 0.4/\zeta = 6.4$.

When we continue to make the condensate evolve in time, the vortex lattice structure of condensate begins to be randomly arranged as shown in Figure 8 and suggested in [4].

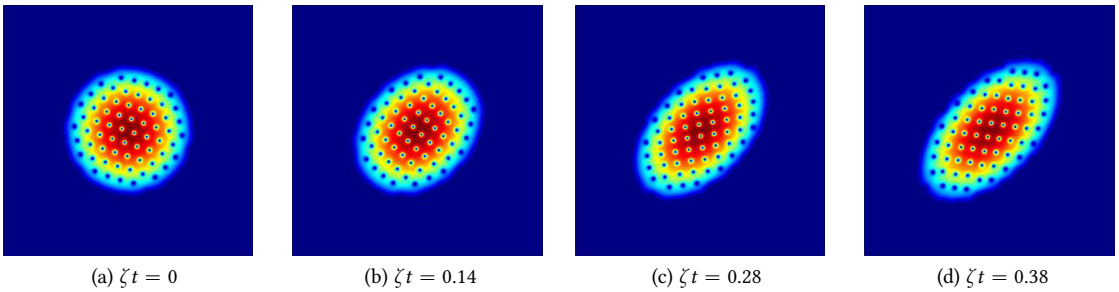

(a) $\zeta t = 0$ (b) $\zeta t = 0.14$ (c) $\zeta t = 0.28$ (d) $\zeta t = 0.38$

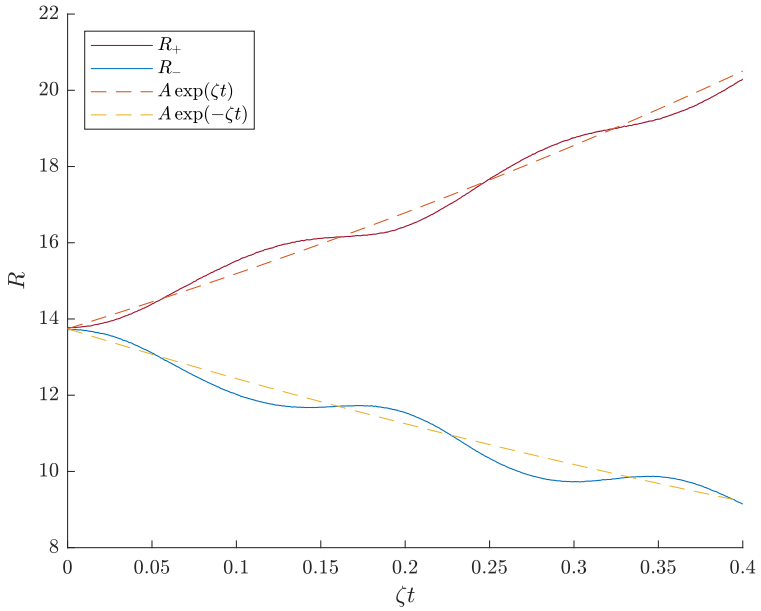

(e)

Figure 7: (a-d) plots of the state density $|\Psi(x, y, t)|^2$ of squeezed condensate at the time $\zeta t = 0, 0.14, 0.28$ and 0.38; (e) plot of time evolution of the major and minor of cloud radii $R_\pm$ scaled by $\ell_B = \sqrt{\hbar/(2m\omega_x)}$ not by $\ell = \sqrt{\hbar/(m\omega_x)}$. We use MATLAB's Image Processing Toolbox to determine these radii. The dashed lines are the exponential fits $A\exp(\pm\zeta t)$ as suggested in [15] in which A is a free parameter chosen as the average of the major and minor radii at $\zeta t = 0$.

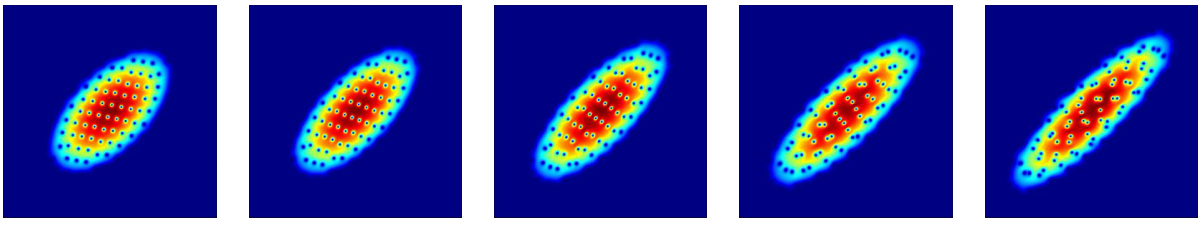

(a) $\zeta t = 0.40$ (b) $\zeta t = 0.45$ (c) $\zeta t = 0.50$ (d) $\zeta t = 0.55$ (e) $\zeta t = 0.60$

Figure 8: Plots of the state density $|\Psi(x, y, t)|^2$ of squeezed condensate at the time $\zeta t = 0.40, 0.45, 0.50, 0.55$ and 0.60.

6 Conclusion

Numerically solving non-linear equations like the Gross-Pitaevskii equation is a time-consuming process with most methods [8], especially for rotating Bose-Einstein condensates. In addition to high computational cost, they may be

unsuccessful to find the ground state due to the existence of many local minima in energy. Hence, we prefer to use the multigrid preconditioned Polak–Ribière–Polyak conjugate gradient method [12] which is more efficient and easy-to-apply compared with those. With this method, we can find a feasible ground state of Bose-Einstein condensates much easier and faster even in the case of $Ng \gg 1$ and/or $\Omega \to 1$ as shown in Section 4. Since the aim of this project is to reproduce the results of the experiment on the geometric squeezing in a Bose-Einstein condensate conducted by Martin Zwierlein's research group, we first try to calculate the ground state. Due to making the approximation of 2D coupling constant g by reducing the 3D Gross-Pitaevskii equation to 2D as in Section 5.1, the number of vortices in the numerical result turns out to be higher than the one in the experiment.

After getting a similar ground state, a new potential, namely, the saddle potential is applied at $\Omega = 1$ for a while by using the time-splitting spectral method [5, 8]. The numerical result indicates that squeezing occurs in both the lattice structure and cloud shape of the condensate as expected in [15]. We also observe the oscillations in the cloud radii and the breakdown of the vortex lattice structure as suggested in the experiment.

For future work, one can focus on the slight inconsistency in the number of vortices. This problem may be solved by finding a more proper way to approximate the 2D coupling constant for 3D systems.

References

[1] C. Samuelis, E. Tiesinga, T. Laue, M. Elbs, H. Knöckel, and E. Tiemann, Phys. Rev. A **63**, 012710 (2000).

[2] J. R. Abo-Shaeer, C. Raman, J. M. Vogels, and W. Ketterle, Science **292**, 476 (2001).

[3] K. W. Madison, F. Chevy, V. Bretin, and J. Dalibard, Phys. Rev. Lett. **86**, 4443 (2001).

[4] P. Engels, I. Coddington, P. C. Haljan, and E. A. Cornell, Phys. Rev. Lett. **89**, 100403 (2002).

[5] W. Bao, D. Jaksch, and P. A. Markowich, Journal of Computational Physics **187**, 318 (2003).

[6] K. Kasamatsu, M. Tsubota, and M. Ueda, Phys. Rev. A **67**, 033610 (2003).

[7] A. Aftalion, X. Blanc, and J. Dalibard, Phys. Rev. A **71**, 023611 (2005).

[8] W. Bao and H. Wang, Journal of Computational Physics **217**, 612 (2006).

[9] A. L. Fetter, Phys. Rev. A **75**, 013620 (2007).

[10] C. J. Pethick and H. Smith, *Bose–einstein condensation in dilute gases*, 2nd ed. (Cambridge University Press, 2008).

[11] A. Kato, Y. Nakano, K. Kasamatsu, and T. Matsui, Phys. Rev. A **84**, 053623 (2011).

[12] X. Antoine, A. Levitt, and Q. Tang, Journal of Computational Physics **343**, 92 (2017).

[13] R. H. Petrucci, F. G. Herring, J. Madura, and C. Bissonnette, *General chemistry: principles and modern applications*, 11th ed. (Pearson, 2017).

[14] X. Antoine, Q. Tang, and Y. Zhang, Communications in Computational Physics **24**, 10.4208/cicp.2018.hh80.11 (2018).

[15] R. J. Fletcher, A. Shaffer, C. C. Wilson, P. B. Patel, Z. Yan, V. Crépel, B. Mukherjee, and M. W. Zwierlein, *Geometric squeezing into the lowest landau level*, 2019.